minerals

MDPI

Article

Stability of Naturally Relevant Ternary Phases in the Cu–Sn–S System in Contact with an Aqueous Solution

Andrea Giaccherini [1], Giordano Montegrossi [2,*] and Francesco Di Benedetto [2,3]

[1] Department of Chemistry, University of Florence, via della lastruccia 3, Sesto Fiorentino 50019, Italy; andrea.giaccherini@unifi.it

[2] National Research Council, Institute for Geosciences and Georesources, via G. La Pira 4, Firenze 50121, Italy

[3] Department of Earth Sciences, University of Florence, via G. La Pira 4, Firenze 50121, Italy; francesco.dibenedetto@unifi.it

* Correspondence: montegrossi@igg.cnr.it; Tel.: +39-55-275-7495

Academic Editor: Federica Zaccarini

Received: 9 June 2016; Accepted: 22 July 2016; Published: 26 July 2016

Abstract: A relevant research effort is devoted to the synthesis and characterization of phases belonging to the ternary system Cu–Sn–S, mainly for their possible applications in semiconductor technology. Among all ternary phases, kuramite, Cu_3SnS_4, mohite, Cu_2SnS_3, and $Cu_4Sn_7S_{16}$ have attracted the highest interest. Numerous studies were carried out claiming for the description of new phases in the ternary compositional field. In this study, we revise the existing literature on this ternary system, with a special focus on the phases stable in a temperature range at 25 °C. The only two ternary phases observed in nature are mohite and kuramite. Their occurrence is described as very rare. A numerical modelling of the stable solid phases in contact with a water solution was underwent to define stability relationships of the relevant phases of the system. The numerical modelling of the Eh-pH diagrams was carried out through the *phreeqc* software with the lnll.dat thermodynamic database. Owing to the complexity of this task, the subsystems Cu–O–H, Sn–O–H, Cu–S–O–H and Sn–S–O–H were firstly considered. The first Pourbaix diagram for the two naturally relevant ternary phases is then proposed.

Keywords: Cu–Sn–S system; kuramite; mohite; thermodynamics; pourbaix diagrams

1. Introduction

Recent studies have pointed out interesting semiconducting performances in some terms of the ternary Cu–Sn–S system [1–5]. Namely, Cu_3SnS_4, Cu_2SnS_3 and Cu_4SnS_4 are considered as novel materials for the p-layer of thin film technology in solar energy conversion devices. Their energy gap and absorption coefficient, coupled to the fact that they consist of cheap and abundant elements, are studied as materials for next-generation thin film solar cells under the scheme of the thin film technology, together with other materials as the kesterite and $CuZnSn(S,Se)_4$. Moreover, the thermoelectric features of Cu_2SnS_3 and $Cu_4Sn_7S_{16}$ are also considered for the realization of new thermoelectric devices [4].

The economic exploitation of these substances in their future application asks for accurate knowledge about their stability in relation to the possible use. For instance, photovoltaic devices have to cycle, with a daily period, in a relatively wide temperature range, and should maintain their good performances over time. A second challenge is represented by the synthetic way to obtain them. These materials are usually synthesized by means of energy consuming pathways, requiring vacuum conditions, long run duration and high annealing temperatures. To minimize the energy costs of the synthesis, the research is moving towards mild hydro- and solvothermal approaches (e.g., [6,7]).

The present study is aimed to revise all information available on the ternary Cu–Sn–S system, and to explore the contribution that the thermodynamic modeling of the interaction of binary and ternary sulfide phases with a water solution could add to the knowledge about stability of these technologically relevant materials. The paper is organized as follows: in Section 2, a summary of the stability relationships in the ternary compositional field is provided; in Section 3, the details of the modeling are discussed; in Section 4, the numerical modeling is performed on some test systems (Cu–O–H, Sn–O–H, Cu–S–O–H, Sn–S–O–H); and, in Section 5, the results of the numerical modeling of the Cu–Sn–S–O–H system, not present in the literature, is reported.

2. State-of-the-Art in the Cu–Sn–S Compositional Field

The ternary Cu–Sn–S system and some of its most relevant pseudobinary joins have attracted a relevant interest during the 1970s, and then repeatedly studied [8–25]. Most of these studies focused on the Cu_2S–SnS_2 pseudobinary join, whose definitive assessment dates to Olekseyuk et al. [23]. Other pseudobinary joins (Cu_2S–SnS, Cu_2S–Sn_2S_3) were investigated by Khanafer et al. [10], whereas an isotherm section at 500 °C is due to Wu et al. [19].

Numerous phases were reported to occur in this system during more than 40 years of research. They are listed in the Table 1, together with their lower limits of the stability field. It is worth mentioning that a careful reconsideration of the existing literature leads to a reduction of the total number of phases. In the past, in fact, successive studies, carried out in phases of the ternary system, reported different chemical formulas, while describing the same crystalline phase [1]. This fact holds particularly true for the phases labelled as "c" and "d" in Table 1. "c" phases refer to the one corresponding to the formula $Cu_2Sn_4S_9$ [23] or $Cu_4Sn_7S_{16}$ [25]. For all phases belonging to the "c" group, Fiechter et al. [24] suggests that they could be represented by a small compositional field (at $T > 500$ °C) described by a general law: $Cu_2Sn_{3+x}Sn_{7+2x}$, which will also include the $Cu_2Sn_4S_9$ composition. "d" phases refer to the one corresponding to the formula Cu_4SnS_6. On the whole, the number of phases still considered valid in the Cu–Sn–S system reduces to six (corresponding to the a–f groups in Table 1). During the evolution of the knowledge about the stability fields in this system, some other phases were identified and successively discredited (see notes to Table 1).

Table 1. Phases of the Cu–Sn–S system described in the literature.

#	Formula	Lower Limit of the Stability Field	Reference(s)
a	Cu_4SnS_4	RT	[8,12,14,18,22,23]
b	Cu_2SnS_3	RT	[8,12,13,18,22,23]
c	$Cu_2Sn_4S_9$	RT	[9,22,23]
	$Cu_2Sn_3S_7$		[8,10,18,23]
	$Cu_2Sn_{3.5}S_8$		[12,23]
	$Cu_2Sn_{3.75}S_8$		[23]
	$Cu_2Sn_{3.34}S_{7.68}$		[12]
	$Cu_4Sn_7S_{16}$		[20,24]
d	$Cu_{10}Sn_2S_{13}$	400 °C	[18,23]
	$Cu_{9.67}Sn_{2.33}S_{13}$		[11,18,23]
	Cu_4SnS_6		[15,21,23]
e	$Cu_5Sn_2S_7$	600 °C	[13,18,23]
f	$Cu_7Sn_3S_{10}$	600 °C	[13,18,23]
g	Cu_3SnS_4	RT *	[16,23]

Other phases claimed to occur in the ternary Cu–Sn–S system but successively discredited: $Cu_4Sn_3S_8$ [22]; $Cu_2Sn_2S_5$ [18]; Cu_5SnS_4 [18]. * The stability of Cu_3SnS_4 was tested as this is a product of spontaneous reaction between Cu_4SnS_4 and S at $T < 300$ °C. RT, room temperature.

According to the most recent studies [19,23,24], only three ternary Cu–Sn–S compounds are stable at room temperature, i.e., Cu_4SnS_4, Cu_2SnS_3 and $Cu_2Sn_4S_9$ (Figure 1). Interestingly, they all belong to the pseudobinary join Cu_2S–SnS_2. In addition to the previously cited phases, high temperature terms are reported in the Figure 1: Cu_4SnS_6, above 400 °C, $Cu_5Sn_2S_7$ and $Cu_{10}Sn_2S_{13}$, above 500 °C.

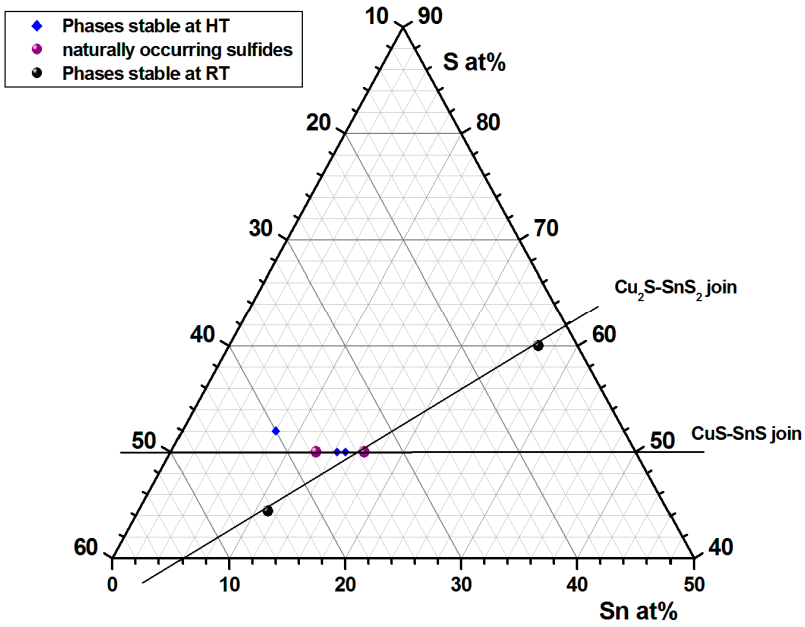

Figure 1. Ternary Cu–Sn–S system, reporting the phases found in nature (purple spheres), those reported as stable at room temperature (RT, black spheres) and those reported as stable at temperature values > 400 °C (HT, high temperature, blue diamonds).

A further relevant point resides in the consideration that none of the six cited phases are naturally occurring, except for Cu_2SnS_3. This latter phase corresponds to the mineral mohite. This mineral has been firstly described by Kovalenker et al. [26] and it was found in hydrothermal vein deposits (e.g., at Barquilla, Salamanca, Spain [27]) or associated with gold/silver deposits, included in sulfostannate assemblages (still of hydrothermal origin, at about 300–350 °C [28]). A peculiar case is represented by Cu_3SnS_4, kuramite, corresponding to the seventh group in Table 1. This phase represents the unique other naturally occurring ternary phase. Kuramite was firstly described by Kovalenker et al. [29], and it has also been reported in hydrothermal deposits, either in association with mohite (e.g., in gold-silver deposits [28]) or not (as e.g., at Agua Rica, Catamarca, Argentina [30,31]). The stability range of kuramite was studied on synthetic samples by Wang [17], who found it stable below 300 °C. This temperature range was studied through sulfidisation of Cu_4SnS_4 (i.e., through an out-of-equilibrium synthetic approach).

3. Modelling of the Equilibria in Aqueous Solutions

In the present study, the relationships between the main phases of the Cu–Sn–S system and a water solution are studied through the use of Eh versus pH (or "*Pourbaix*") diagrams, calculated according to the point-by-point mass balance method [32]. Under this approach, the predominant species at each given point of Eh and pH can be identified, taking into account other variables, as presence of ligand(s), temperature and pressure [32]. The predominant species is identified as the species with the highest content of the considered element. This predominance involves the absolute element content (in moles) considering both aqueous and solid species.

We performed our point-by-point mass balance calculation under the *phreeqc* formalism [33,34]. Aqueous phase equilibria are taken into account in a reference database file and the solid phases are

included through dissolution/precipitation reactions and reported as the logarithm of equilibrium constant (log K) at standard temperature and pressure condition (i.e., 25 °C and 1.0132 bar) [35,36]. Then, a Jacobian matrix including all the mass balance constants relative to the master species (Cu, Sn, S, H, O) is diagonalized obtaining the concentrations that satisfy the simultaneous solutions to all the considered equilibria.

Solid Phases Considered in the Calculations

Geochemical numerical models require comprehensive thermodynamic databases. Although today's geochemical databases are quite complete, including the most common reactions and reaction constants, some equilibria typical of specific environments may be not present. Accordingly, the thermodynamic properties of some minerals relevant to our model have been checked, and eventually added, to the *phreeqc* wateq4f.dat [37], and llnl.dat, for Sn, databases [38]. For the solid Cu oxides (cuprite, Cu_2O, and tenorite, CuO), calculations were performed using two different internally consistent sets of log K, one from the wateq4f.dat database [37], and the other from the JANAF tables [39]. The thermodynamic constants of the binary sulfides (chalcocite, Cu_2S, and covellite, CuS) arise from the wateq4f.dat database [37,40]. We included chalcocite, covellite and the crystalline defect $Cu_{2-x}S$ sulfides, i.e., djurleite, digenite and anilite.

A more detailed discussion deals with the ternary sulfide phases. As evinced from the previous paragraph, only two ternary phases, namely kuramite and mohite, are naturally relevant. Thus, we focused, in the calculation, only on these phases. However, experimental thermodynamic studies of mohite are lacking. Owing to this fact, an estimation of its log K respect to solvated ions is needed to refer to the *phreeqc* formalism and to evaluate their stability in contact with a solution.

A way to estimate the enthalpy of formation of mohite consists in obtaining it through the use of a Born-Haber cycle. The simplest way of designing a proper cycle should include the known binary compounds, as chalcocite, covellite, berndtite (SnS_2) and herzenbergite (SnS) and kuramite. However, starting from the binary sulfides, there is no chance of designing a cycle without including a phase in which disulfide groups are included. From a structural point of view, no disulfide groups are present in kuramite [7] nor in mohite [21]. This consideration rules out the possibility to extrapolate thermodynamic properties of the Cu–Sn–S ternary sulfides from the opportune mixing of those of the binary sulfides.

Since thermodynamic properties of crystals are strongly structure-dependent [41,42], we established a Born-Haber cycle including a close structural control on the mineral phases. This cycle is based on the thermodynamic properties of kesterite, Cu_2ZnSnS_4 [43], and kuramite. In kesterite, kuramite and mohite the crystal structure is organized on the same structural type, i.e., the tetrahedral arrangement of all cations within the framework derivative of that of sphalerite (ZnS) [44]. Thus, a close structural similarity between these phases is apparent. Following an approach similar to the linear additivity procedures developed by Yves Tardy and colleagues for other mineral types (e.g., [45,46]), the overall enthalpy of formation of kesterite can be hypothesized as consisting of the sum of the four MS_4 fragments (M = Cu, Zn, Sn). However, this should be done with some additional care due to the heterogeneity of sulphide structures, which may generate strong differences in group energy. In this context, an esteem of the enthalpy of formation of the ZnS_4 fragment can be obtained from the thermodynamic data of sphalerite, which also exhibit an arrangement of tetrahedrally coordinated Zn ions. Similarly, the enthalpy of formation of the SnS_4 fragment can be estimated from a cubic SnS polymorph, isostructural to sphalerite [47].

Accordingly, the enthalpy of formation of mohite can be derived from that of kesterite by subtracting the contribution due to the ZnS_4 fragment, or from that of kuramite by subtracting a CuS_4 fragment. Starting from kuramite, one has to first calculate the enthalpy of formation of a nominal cubic CuS phase having a sphalerite crystal structure, according to the following equation:

$$3\Delta H_{\text{-cub. } CuS_4\text{-}} = \Delta H_{Cu_3SnS_4} - \Delta H_{SnS} \quad (1)$$

and then perform a summation of the CuS_4 and SnS_4 fragments in the opportune ratio. Thus, a Born-Haber cycle involving a hypothetical cubic CuS species can be performed in order to calculate the enthalpy of formation of mohite, and a similar procedure could be done starting from kesterite to check the consistency of the resulting values. We assume that the difference in mixing enthalpies for the three considered multinary compounds (kesterite, kuramite and mohite) is negligible [48]. The log k of formation of mohite is reported in Table 2. The data are in a good agreement with those evinced by the Zawadzki et al. [1] study. The discrepancies are in the range of 15%–20%, and they could be considered small if taking into account a non-homogeneous source for the thermodynamic data.

Table 2. Calculated log K for the dissolution reactions of the ternary species considered in this study.

Mineral	Log K	Reference
Cu_3SnS_4, kuramite	−73.14	This study, wateq4f.dat [37]
Cu_2SnS_3, mohite	−58.03	This study

4. Test Systems (Cu–O–H, Sn–O–H, Cu–S–O–H, Sn–S–O–H)

The predominance charts discussed in the following were computed in a grid limited by the water stability field from 0 to 14 pH units. The choice of the concentration of the master species (Cu, Sn, S) were dictated by the possibility of an immediate comparison with selected Pourbaix diagrams available in the literature. We used as reference diagrams those reported in the two Eh-pH atlantes by Brookins [49] and Takeno [50]. It is noteworthy to mention that the former refer to calculations performed in the "line method" [32], whereas the latter presents results obtained in the mass balance method, using up to five different databases.

Figure 2a shows the Eh-pH diagram for Cu in water. There is an almost perfect agreement between our diagram and that proposed by [49] and by [32]. If compared to those presented by [50], the major differences reside in the decrease of the stability field of cuprite, and in the appearance of a field or Cu^+. Both of these effects can be related to the different concentration used by these authors ([Cu] = 10^{-6} and 10^{-10} mol/kgw). To verify this, we performed a calculation under their assumptions, still obtaining an excellent agreement. The comparison of diagrams obtained by different methods can yield slight differences in the boundaries as well as in the identification of the predominant species, and this can be due to the number and type of equilibria involved in the calculations [51]. In the present case, one has to highlight the presence (at high pH values) of a stability field of the $Cu(OH)_4^{2-}$ aqueous species, in perfect agreement with [32]: this field is not cited by [49] and [50], where a similar field was assigned to CuO_2^{2-}.

The Eh-pH diagram for Sn in water, shown in the Figure 2b, matches with a good agreement the data reported by [49]. Most of the diagram is dominated by cassiterite. The major differences reside in the absence of stability field of dissolved species at very low pH values (pH < 0.5) in the Brookins' [49] diagram. A better agreement is observed with the diagrams proposed by [50], even taking into account the difference in concentration. Again, we performed a calculation assuming [Sn] = 10^{-10} mol/kgw, verifying an almost excellent agreement. The major difference between our diagram and that proposed by [49] can be attributed to the fact that in its line diagram, only few equilibria involving hydroxide complexes of Sn^{2+} were included, equlibria that are considered by our and Takeno's [50] calculations. The role of the complexing equilibria can obviously shift the boundaries between solid and aqueous species (as verified for the HS^- ligand by [44]). In contrast, both the line and mass balanced diagrams by [49,50] agree in pointing out a small field at negative Eh and high pH, where a soluble Sn^{2+} complex is more stable than cassiterite.

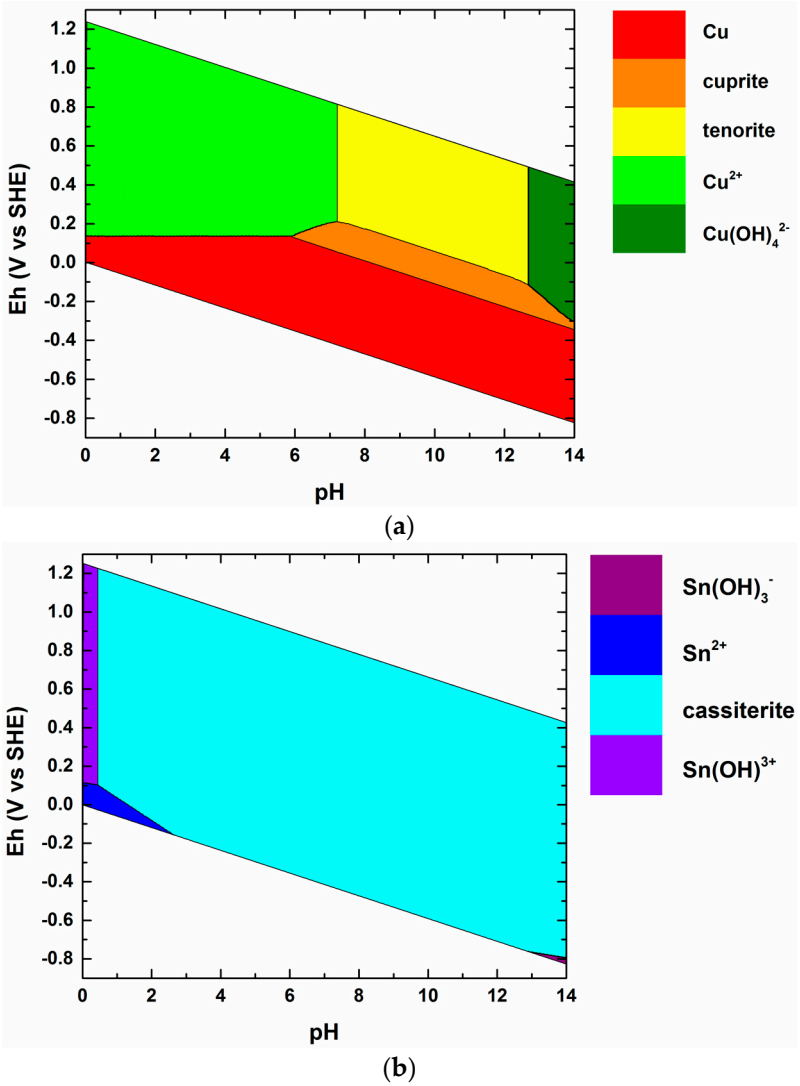

Figure 2. Eh-pH diagrams of: (**a**) the Cu–O–H system, calculated assuming [Cu] = 10^{-6} mol/kgw; (**b**) the Sn–O–H system, calculated assuming [Sn] = 10^{-8} mol/kgw.

Figure 3a depicts the diagram for the Cu–S system in water. In this case, the agreement of our calculation with the numerous available diagrams in the literature (e.g., [32,49,51,52]) is excellent, almost independently of the type of calculation (line or mass balanced methods) of the cited references. Concerning the defect $Cu_{2-x}S$ species, they were not included in Brookins' [49] calculations, but the present results fully agree with the fields proposed by the other authors. Concerning the results proposed by Young et al. [50], a marked difference regards the fields of the Cu(I) and Cu(II) thiocomplexes, which were not included in the present calculations (we reputed this detail beyond the aims of the present study). As already stated, the role of these thiocomplexes was revealed to be of some relevance in the definition of the proper stability fields and boundaries in the metal–sulfur–water Pourbaix diagrams [50].

Concerning the Sn–S–O–H– system, an exemplar diagram is shown in the Figure 3b. To the authors' knowledge, the unique reference diagram is provided by [49]. A good agreement between the two diagrams is observed: the diagram is dominated by the cassiterite stability field, limited at low pH values (pH < 0.5) by $Sn(OH)^{3+}$, and at high pH, low Eh values (pH > 13) by $Sn(OH)_3^-$. The remarkable difference with respect to the Sn–O–H system is the comparison of a large stability field for berndtite, while no herzenbergite fields are observed. A marked difference between our and

Brookins' [49] diagrams is the occurrence in the present calculation of a stability field for $SnSO_4$. Again, this fact is ascribed to the absence of this species in the calculations performed by [49].

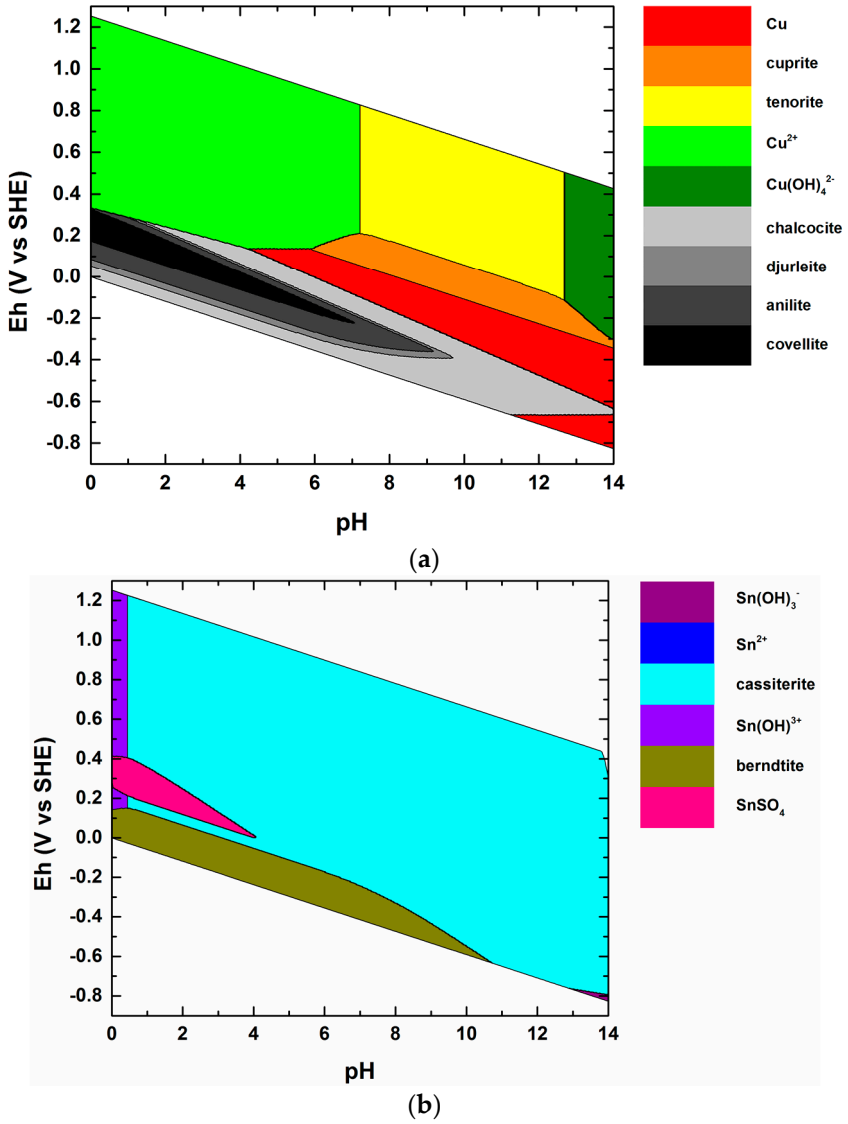

Figure 3. Eh-pH diagrams of: (**a**) the Cu–S–O–H system, calculated assuming [Cu] = 10^{-6} mol/kgw and [S] = 10^{-3} mol/kgw; (**b**) the Sn–S–O–H system, calculated assuming [Sn] = 10^{-8} mol/kgw and [S] = 10^{-3} mol/kgw.

5. The Study of the Cu–Sn–S–O–H System

The Eh-pH diagram for the Cu–Sn–S–O–H system (Figure 4) was calculated holding the 1:1 ratio between the initial concentrations of the metals ([Cu] = [Sn] = 10^{-6} mol/kgw) and choosing 10^{-3} mol/kgw for [S], to let the graph comparable with those already presented in this study (i.e., Figures 2a and 3a). Only minor differences are observed comparing the Figures 3a and 4a. They mainly reside in a small increase of the covellite predominance field. Comparing the Figures 3b and 4b, the main differences consist in the disappearance of the fields relative to the species in solution at pH < 0.5 and pH > 13. Both fields are replaced by cassiterite. This change is not due to the different system analyzed, but it could be ascribed to the change in Sn concentration. In fact, at least under the adopted conditions for the calculations, the two systems Cu–S–O–H and Sn–S–O–H can be considered as

independent, owing to the fact that the ligand species (i.e., OH^-, HS^- and SO_4^{2-}) are abundant with respect to the concentration of Cu and Sn.

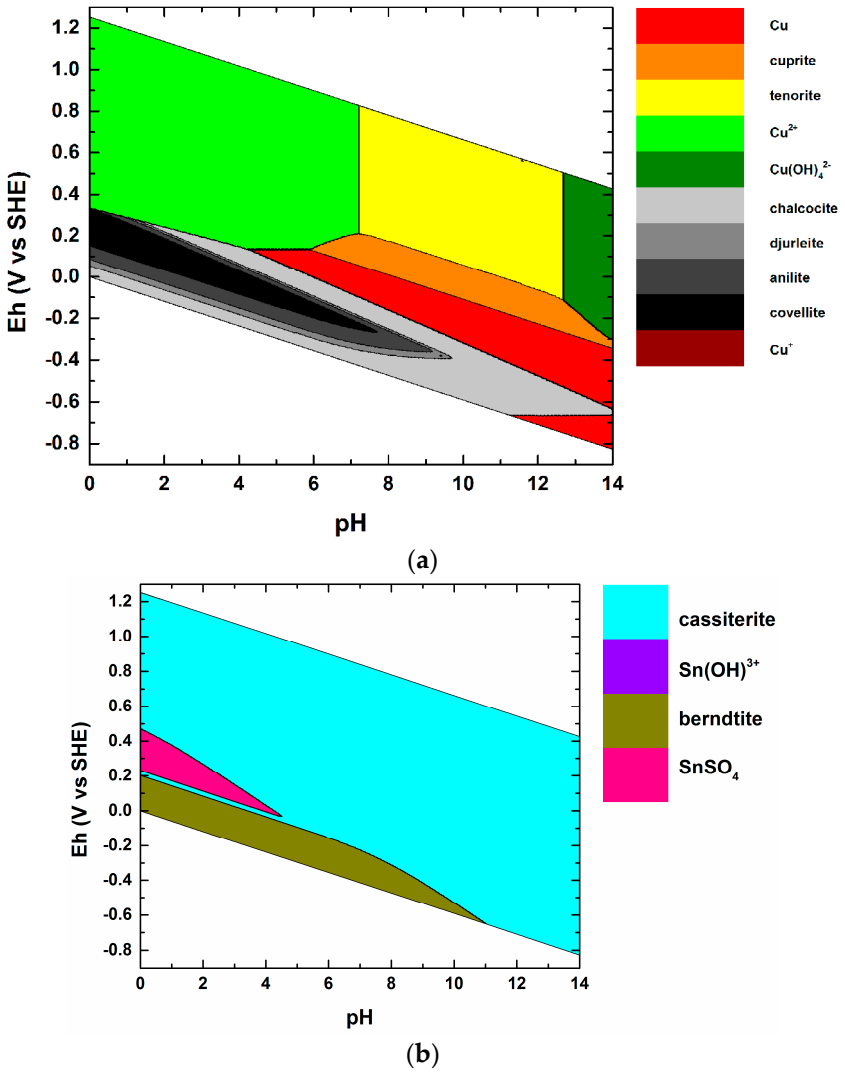

Figure 4. Eh-pH diagrams of the Cu–Sn–S–O–H system, calculated assuming [Cu] = 10^{-6} mol/kgw, [Sn] = 10^{-6} mol/kgw and [S] = 10^{-3} mol/kgw. (**a**) Diagram for the Cu species; (**b**) diagram for the Sn species.

A remarkable consideration point to the absence of predominance fields for either kuramite or mohite. This means that, at room temperature, these two minerals never attain a condition where they become the prevailing species in the system. This does not necessarily imply that the two minerals do not have a stability field at room temperature. For this reason, the stability fields of mohite and kuramite were plotted in Figure 5a,b, respectively. These fields were obtained allowing only mohite (or kuramite) to precipitate. The other, eventually concurring, precipitation mechanisms were not included in the mass balance. Accordingly, the fields reported in the Figure 5 represent the maximum stability field obtainable for the given mineral species, given the external (temperature, pressure, batch chemical composition) conditions. In the two figures, the black and red fields represent the stability field evaluated with respect to the Cu and Sn species, respectively. Accordingly, as mohite and kuramite are ternary compounds, both conditions have to be simultaneously satisfied. The actual stability field for mohite and kuramite are thus defined by the red (intersection) boundaries. Figure 5 is pointing to a definitely wider stability field for mohite than for kuramite, which is found stable

only in a limited range of Eh and pH. In contrast, mohite appears to be stable over a field more or less equivalent to that of chalcocite, which, of course, is always prevailing in terms of precipitated amount (in an unconstrained system, Figure 4a). Specific punctual tests carried out with *phreeqc* have verified that a subordinate amount of mohite is always occurring in association to the phases of the Cu–S system, in their stability fields of Figure 4a. It is worth mentioning that the partial superposition of the two stability fields is in a very good agreement with the evidence of coupled occurrence of the minerals in the low temperature hydrothermal genetic environment.

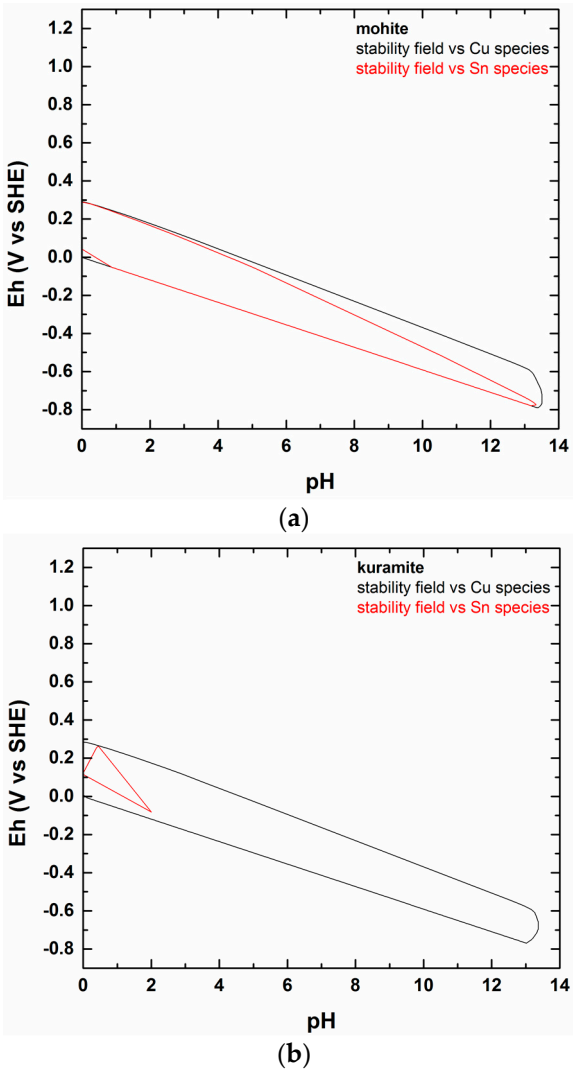

Figure 5. Stability fields for mohite (**a**) and kuramite (**b**) evaluated with respect to the Cu (**black** boundaries) and Sn (**red** boundaries) species. The calculation conditions are the same of the Figure 5.

The main result of this numerical modelling deals with the instability of the two phases, at room temperature, when kept in contact with a water solution. The presence of water, in fact, would favor their reaction towards more stable phases, as e.g., Cu and Sn binary sulfides. This fact has a fundamental consequence for application of these materials in technological devices, as their use has to be maintained in a water/moisture free environment. Similarly, we can expect that hydrothermal syntheses of mohite and kuramite will be less effective in providing good nanoparticle materials, than solvothermal syntheses.

6. Conclusions

The present study summarizes the state of the art concerning the stability of the ternary phases described in the Cu–Sn–S system. Moreover, a preliminary description of their stability at room temperature and pressure conditions is provided. According to our evaluation, mohite and kuramite, the only ternary Cu–Sn–S phases found in nature, can be considered relatively stable if under anhydrous conditions, and their presence in a mineral assemblage can be used to assess not only the temperature but also the Eh-pH window of precipitation.

As far as the materials science is concerned, our results can be considered at least in line with most of the synthetic results, who obtained kuramite and mohite preferring the solvothermal environment [2,6,7].

We are aware that this study is only preliminary, and future steps will involve the evaluation of the stability fields for the two minerals in relation to the temperature variable in a range from 25 to 350 °C, and the extension of the Eh-pH analysis also to non aqueous environment, to fully describe the solvothermal precipitation.

Acknowledgments: This manuscript was funded by the ex 60% 2013 (Department of Earth Sciences, University of Florence) funds to Francesco Di Benedetto.

Author Contributions: Giordano Montegrossi conceived and designed the numerical modelling strategy; Giordano Montegrossi and Andrea Giaccherini performed the *phreeqc* modelling; Francesco Di Benedetto conceived and realized the revision of the literature of the Cu–Sn–S system. All authors equally contributed to the interpretation of the results and to the development and writing of its sections.

Conflicts of Interest: The authors declare no conflict of interest.

References

1. Zawadzki, P.; Baranowski, L.L.; Peng, H.; Toberer, E.S.; Ginley, D.S.; Tumas, W.; Zakutayev, A.; Lany, S. Evaluation of photovoltaic materials within the Cu–Sn–S family. *Appl. Phys. Lett.* **2013**, *103*, 253902. [CrossRef]
2. Tipcompor, N.; Thongtem, S.; Thongtem, T. Effect of microwave radiation on the morphology of tetragonal Cu_3SnS_4 synthesized by refluxing method. *Superlattices Microstruct.* **2015**, *85*, 488–496. [CrossRef]
3. Chen, Y.; Ma, L.; Yin, Y.; Qian, X.; Zhou, G.; Gu, X.; Liu, W.; Wu, X.; Zhang, F. Strong quantum confinement effect in Cu_4SnS_4 quantum dots synthesized via an improved hydrothermal approach. *J. Alloy. Compd.* **2016**, *672*, 204–211. [CrossRef]
4. Tan, Q.; Sun, W.; Li, Z.; Li, J.-F. Enhanced thermoelectric properties of earth-abundant Cu_2SnS_3 via in doping effect. *J. Alloy. Compd.* **2016**, *672*, 558–563. [CrossRef]
5. Baranowski, L.L. Combinatorial Development of Cu2SnS3 as an Earth Abundant Photovoltaic Absorber. Ph.D. Thesis, Colorado School of Mines, Golden, CO, USA, 2015. p. 143.
6. Lokhande, A.C.; Gurav, K.V.; Jo, E.; Lokhande, C.D.; Hyeok Kim, J. Chemical synthesis of Cu_2SnS_3 (CTS) nanoparticles: A status review. *J. Alloy. Compd.* **2016**, *656*, 295–310. [CrossRef]
7. Di Benedetto, F.; Bencistà, I.; D'Acapito, F.; Frizzera, S.; Caneschi, A.; Innocenti, M.; Lavacchi, A.; Montegrossi, G.; Oberhauser, W.; Romanelli, M.; et al. Geomaterials related to photovoltaics: A nanostructured Fe-bearing kuramite, Cu_3SnS_4. *Phys. Chem. Miner.* **2016**, *2016*, 1–10. [CrossRef]
8. Moh, G.H. Tin-containing mineral systems. Part I: The Sn–Fe–S–O system and mineral assemblages in ores. *Chemie Der Erde* **1974**, *33*, 243–273.
9. Wang, N. The three ternary phases in the system Cu–Sn–S. *N. Jb. Miner. Mh.* **1974**, *9*, 424–431.
10. Khanafer, W.; Rivet, J.; Flahaut, J. Etude du ternaire Cu–Sn–S. Diagrammes d'equilibre des systémes Cu_2S–SnS, Cu_2S–Sn_2S_3 et Cu_2S–SnS_2. Etude cristallographique des composés Cu_4SnS_4, Cu_2SnS_3, $Cu_2Sn_4S_9$, et $Cu_4Sn_3S_8$. *Bull. Soc. Chem. France* **1974**, *12*, 267–276. (In French)
11. Moh, G.H. Tin-containing mineral systems. Part II: Phase relations and mineral assemblage in the Cu–Fe–Zn–S system. *Chemie Der Erde* **1975**, *34*, 1–61.
12. Wang, N. Idaite and the synthetic phases $Cu_{4.33}Ge_{0.67}S_5$ and $Cu_{9.67}Sn_{2.33}S_{13}$. *N. Jb. Miner. Mh.* **1976**, *1976*, 241–247.

13. Sobott, R.J.G.; Teh, G.H. Investigations along the Cu_2S–SnS_2 join in the Cu–Sn–S system. *N. Jb. Miner. Abh.* **1977**, *131*, 23–26.
14. Wang, N. Structural variations of non-stoichiometric Cu_2SnS_3. *N. Jb. Miner. Abh.* **1977**, *131*, 26–27.
15. Jaulmes, S.; Rivet, J.; Laruelle, P. Cuivre–Etain–Soufre Cu_4SnS_4. *Acta Cryst. B Struct. Crystallogr. Cryst. Chem.* **1977**, *33*, 540–542. [CrossRef]
16. Wang, N. Covellite related phases within the Cu–Fe–Sn–S system. *N. Jb. Miner. Mh.* **1981**, *1981*, 337–343.
17. Wang, N. Sulfidization experiments performed at low temperatures. *N. Jb. Miner. Abh.* **1982**, *144*, 319–324.
18. Jaulmes, J.; Rivet, J.; Jumas, M. Structure Cristalline du Sulfure et D'Etain $CuSn_{3,75}S_8$. *Acta Cryst. B Struct. Crystallogr. Cryst. Chem.* **1982**, *38*, 51–54. (In French) [CrossRef]
19. Wu, D.; Knowles, C.R.; Chang, L.L.Y. Copper-tin sulphides in the system Cu–Sn–S. *Miner. Mag.* **1986**, *50*, 323–325. [CrossRef]
20. Osadchii, E.G. Solid solutions kesterite–Mn–stannite and sphalerite–alabandite in the pseudoternary system Cu2SnS3–ZnS–MnS at 820 °C and 700 °C. *N. Jb. Miner. Mh.* **1996**, *6*, 201–211.
21. Chen, X.; Wada, H.; Sato, A.; Mieno, M. Synthesis, Electrical Conductivity, and Crystal Structure of $Cu_4Sn_7S_{16}$ and Structure Refinement of Cu_2SnS_3. *J. Solid State Chem.* **1998**, *139*, 144–151. [CrossRef]
22. Chen, X.; Wada, H.; Sato, A. Preparation, crystal structure and electrical properties of Cu_4SnS_6. *Mater. Res. Bull.* **1999**, *34*, 239–247. [CrossRef]
23. Olekseyuk, I.D.; Dudchak, I.V.; Piskach, L.V. Phase equilibria in the Cu_2S–ZnS–SnS_2 system. *J. Alloy. Compd.* **2004**, *368*, 135–143. [CrossRef]
24. Fiechter, S.; Martinez, M.; Schmidt, G.; Henrion, W.; Tomm, Y. Phase relations and optical properties of semiconducting ternary sulfides in the system Cu–Sn–S. *J. Phys. Chem. Solids* **2003**, *64*, 1859–1862. [CrossRef]
25. Jemetio, J.P.F.; Zhou, P.; Kleinke, H. Crystal structure, electronic structure and thermoelectric properties of $Cu_4Sn_7S_{16}$. *J. Alloy. Compd.* **2006**, *417*, 55–59. [CrossRef]
26. Kovalenker, V.A.; Malov, V.S.; Evstigneeva, T.L.; Vyal'sov, L.N. Mohite, Cu_2SnS_3, a new sulfide of tin and copper. *Zapiski. Vses. Mineralog. Obshch.* **1982**, *111*, 110–114. (In Russian) [CrossRef]
27. Pascua, M.I.; Murciego, A.; Pellittero, E. Sn–Ge–Gd–Cu–Fe-Bearing Sulfides and Sulfosalts from the Barouilla Deposit, Salamanca, Spain. *Can. Miner.* **1997**, *35*, 39–52.
28. Kovalenker, V.A.; Nekrasov, I.Y.; Malov, V.S. Copper and iron sulfostannate minerals in gold-silver deposits. *Int. Geol. Rev.* **1986**, *28*, 1443–1459. [CrossRef]
29. Kovalenker, V.A. Kuramite, Cu_3SnS_4, a new mineral of the stannite group. *Int. Geol. Rev.* **1981**, *23*, 365–370. [CrossRef]
30. Franchini, M.; Impiccini, A.; O'Leary, S.; Ríos, F.J.; Schalamuk, A.I. Distribución de las alteraciones y mineralizaciones en la sección central del yacimiento Agua Rica (27°22′ S–66°16′ O), Catamarca. *Rev. Asoc. Geol. Argent.* **2009**, *64*, 391–408. (In Spanish)
31. Franchini, M.; Impiccini, A.; Lentz, D.; Ríos, F.J.; O'Leary, S.; Pons, J.; Schalamuk, A.I. Porphyry to epithermal transition in the Agua Rica polymetallic deposit, Catamarca, Argentina: An integrated petrologic analysis of ore and alteration parageneses. *Ore Geol. Rev.* **2011**, *41*, 49–74. [CrossRef]
32. Huang, H.H. The Eh-pH Diagram and Its Advances. *Metals* **2016**, *6*, 23. [CrossRef]
33. Parkhurst, D.L.; Appelo, C.A.J. *User's Guide to PHREEQC (Version 2)—A Computer program for Speciation, Batch-Reaction, One-Dimensional Transport, and Inverse Geochemical Calculations*; Water-Resources Investigations Report 99-4259; U.S. Geological Survey, Earth Science Information Center, Open-File Reports Section: Reston, VA, USA, 1999.
34. Kinniburgh, D.; Cooper, D. PhreePlot: Creating Graphical Output with PHREEQC. Available online: http://nora.nerc.ac.uk/19744/1/PhreePlot.pdf (accessed on 8 June 2016).
35. Helgeson, H.C.; Delaney, J.M.; Nesbitt, H.W.; Bird, D.K. Summary and critique of the thermodynamic properties of rock forming minerals. *Am. J. Sci.* **1978**, *278*, 1–229.
36. Johnson, J.; Oelkers, E.; Helgeson, H. SUPCRT92: A software package for calculating the standard molal thermodynamic properties of minerals, gases, aqueous species and reactions from 1 to 5000 bar and 0 to 1000 °C. *Comp. Geosci.* **1992**, *18*, 899–947. [CrossRef]
37. Ball, J.W.; Nordstrom, D.K. *User's Manual for WATEQ4F, with Revised Thermodynamic Data Base and Text Cases for Calculating Speciation of Major, Trace, and Redox Elements in Natural Waters*; USGS Numbered Series Open-File Report 91-183; U.S. Geological Survey: Reston, VA, USA, 1991; p. 193.

38. Delany, J.M.; Lundeen, S.R. *The LLNL Thermochemical Database: Revised Data and File Format for the EQ3/6 Package*; Lawrence Livermore National Laboratory: Livermore, CA, USA, 1991.
39. Stull, D.R.; Prophet, H. *JANAF Thermochemical Tables*, 2nd ed.; Office of Standard Reference Data, National Bureau of Standards: Washington, DC, USA, 1971; Volume 37, p. 1141.
40. Robie, R.A.; Waldbaum, D.R. *Thermodynamic Properties of Minerals and Related Substances at 298.15 K (25.0 °C) and One Atmosphere (1.013 Bars) Pressure and at Higher Temperatures*; U.S. Government Printing Office: Washington, DC, USA, 1968.
41. Moody, G.J.; Thomas, J.D.R. Lattice energy and chemical prediction: Use of the Kapustinskii Equations and the Born-Haber cycle. *J. Chem. Educ.* **1965**, *42*, 204–210. [CrossRef]
42. Donald, H.; Jenkins, B. Thermodynamics of the Relationship between Lattice Energy and Lattice Enthalpy. *J. Chem. Educ.* **2005**, *82*, 950–952.
43. Jackson, A.J.; Walsh, A. Ab initio thermodynamic model of Cu_2ZnSnS_4. *J. Mater. Chem. A* **2014**, *2*, 7829–7836. [CrossRef]
44. Onoda, M.; Chen, X.; Sato, A.; Wada, H. Crystal structure and twinning of monoclinic Cu_2SnS_3. *Mater. Res. Bull.* **2000**, *35*, 1563–1570. [CrossRef]
45. Vieillard, P.; Tardy, Y. Prediction of enthalpy of formation based on refined crystal structures of multisite compounds. 2. Application to minerals belonging to the system Li_2O-Na_2O-K_2O-BeO-MgO-CaO-MnO-FeO-Fe_2O_3-Al_2O_3-SiO_2-H_2O. Results and discussion. *Geochim. Cosmochim. Acta* **1994**, *58*, 4064–4107. [CrossRef]
46. Vieillard, P. Prediction of enthalpy of formation based on refined cyrstal structures of multisite compounds. 1. Theories and examples. *Geochim. Cosmochim. Acta* **1994**, *58*, 4049–4063. [CrossRef]
47. Burton, L.A.; Walsh, A. Phase Stability of the Earth-Abundant Tin Sulfides SnS, SnS_2, and Sn_2S_3. *J. Phys. Chem. C* **2012**, *116*, 24262–24267. [CrossRef]
48. Baranowski, L.; Zawadzki, P.; Christensen, S.; Nordlund, D.; Lany, S.; Tamboli, A.C.; Gedvilas, L.; Ginley, D.S.; Tumas, W.; Toberer, E.S.; et al. Control of Doping in Cu_2SnS_3 through Defects and Alloying. *Chem. Mater.* **2014**, *26*, 4951–4959. [CrossRef]
49. Brookins, D.G. *Eh-pH Diagrams for Geochemistry*; Springer Science & Business Media: Berlin, Heidelberg, Germany, 1988; p. 176.
50. Takeno, A. *Atlas of Eh-pH Diagrams: Intercomparison of Thermodynamic Databases*; Geological Survey of Japan Open File Report No.419; National Institute of Advanced Industrial Science and Technology, Research Center for Deep Geological Environments: Tokyo, Japan, 2005; p. 285.
51. Young, C.A.; Dahlgren, E.J.; Robins, R.G. The solubility of copper sulfides under reducing conditions. *Hydrometallurgy* **2003**, *68*, 23–31. [CrossRef]
52. Ma, R.; Stegemeier, J.; Levard, C.; Dale, J.G.; Noack, C.W.; Yang, T.; Brown, G.E., Jr.; Lowry, G.V. Sulfidation of copper oxide nanoparticles and properties of resulting copper sulfide. *Environ. Sci. Nano* **2014**, *1*, 347–357. [CrossRef]